Y_2O_3:Bi nanophosphor: Solution combustion synthesis, structure, and luminescence

L. G. Jacobsohn,[a)] M. W. Blair, S. C. Tornga, L. O. Brown, B. L. Bennett, and
R. E. Muenchausen

Los Alamos National Laboratory, Los Alamos, New Mexico 87545, USA

Photoluminescence (PL), radioluminescence (RL), and thermoluminescence (TL) investigation of Y_2O_3:Bi nanophosphors prepared by solution combustion synthesis using urea, glycine, and hexamethylenetetramine (HMT) as fuels was carried out. The as-prepared nanopowders have increasing crystallinity and average crystallite sizes for urea, glycine, and HMT, respectively. Luminescence is composed of two emission bands centered at 408 and 505 nm due to two nonequivalent Bi^{3+} sites with symmetry S_6 and C_2, respectively. The occupancy of these sites depends on the synthesis conditions, in agreement with theoretical predictions. Annealing at 1000 °C for 1 h improves PL and RL efficiency due to enhanced crystallinity of the nanopowders and activation of recombination centers (Bi^{3+} ions). No shift in the PL peak position was observed as a function of average crystallite size. The concentration quenching was experimentally determined to have a maximum emission of around 3 mol % of the dopant. TL spectra present several peaks between 50 and 300 °C, and the total TL signal is correlated with the heat of combustion of the fuel and thus crystallinity increases. Most likely, increases in RL and TL are also due to the increase in the concentration of recombination centers. © *2008 American Institute of Physics*. [DOI: 10.1063/1.3042223]

I. INTRODUCTION

Bi^{3+} ions are commonly used to activate materials, including oxides, phosphates, and borates.[1] These ions have $6s^2$ electronic configuration, with the ground state corresponding to the $^1S_0$ state and the first excited states to $^3P_0$, $^3P_1$, $^3P_2$, and $^1P_1$ for increasing excitation energies.[2] Luminescence from Bi^{3+}-doped materials has been extensively investigated in bulk materials, and a strong dependence on the host was found and ascribed to the coordination characteristics of the activator site, i.e., the number of and distance to ligands.[2,3] The similarity of the ionic radii of Bi^{3+} and Y^{3+} allows for easy substitution of Bi for Y in the Y_2O_3 system and is the focus of this paper. Y_2O_3 has a bcc structure with I/I_c symmetry and there are two six-coordinated nonequivalent cation sites. These sites correspond to atomic configurations where two oxygen vacancies are located on a cube (S_6) or face (C_2) diagonal. The S_6 site presents inversion symmetry and is highly symmetrical; the C_2 site is irregular since there are more atoms on one side of the luminescent center than on the other. Their occupancies are 8 and 24, respectively, out of the 32 sites that comprise the unit cell of Y_2O_3. In Y_2O_3, Bi^{3+} strongly interacts with its surroundings, particularly the first shell of six oxygen ions,[4] and its luminescence is particularly complex in nature due to the existence of the two nonequivalent cation sites. The asymmetric environment of the Bi^{3+} in the host shifts the energy levels, with the Stokes shift increasing for higher asymmetric environments, being 0.31 eV for the S_6 sites and 1.24 eV for the C_2

sites.[5] Two luminescence emission bands have been reported in literature around 410 and 520 nm,[2,3,5–8] which were attributed to the different electronic configurations of the Bi^{3+} ions in the two cation sites.[6,7] The more intense green luminescence was assigned to Bi^{3+} in C_2 sites assuming equal occupancy of these ions in the C_2 and S_6 sites and by taking into account the larger occurrence of C_2 sites.[2] A recent theoretical work that investigated the Bi^{3+} electronic levels in Y_2O_3 in detail using the *ab initio* embedded cluster method coupled with correlated spin-orbit calculations confirmed this assignment.[4] Maximum luminescence efficiency was found for Bi concentrations in the 0.5–2 mol % range.[9]

Recently, the investigation of luminescent properties of nanoscale insulating materials has attracted growing interest in the scientific community. Particular attention has been given to rare-earth doped Y_2O_3, including Eu, Nd, Er, and Tb.[10–13] However, besides considerable investigation of bulk Y_2O_3:Bi, to the best of our knowledge, there are no reports on Y_2O_3:Bi nanophosphor. In this work, the synthesis, structure, photoluminescence (PL), radioluminescence (RL), and thermoluminescence (TL) of this nanomaterial were investigated and compared to the results available in literature for the bulk phosphor.

II. EXPERIMENTAL PROCEDURE

Nanophosphor powders were produced by the solution combustion synthesis (SCS) technique[14,15] using three different organic fuels, urea, glycine, and hexamethylenetetramine (HMT) that have different heats of combustion[16] (Table I). 24 g of Y_2O_3 nanopowder (Alfa Aesar 99.9%, 25–50 nm) were dissolved in an excess of nitric acid (45 ml, Baker,

a)Electronic mail: luizjaco99@hotmail.com. Tel.: (505) 501-0115. FAX: (505) 665-5849.

TABLE I. Relevant information on the combustion conditions and characteristics, including the balancing of $2Y(NO_3)_3 + fuel \rightarrow Y_2O_3 + CO_2 + N_2 + H_2O$ combustion reactions for the production of 1 mol of Y_2O_3.

Fuel	Chemical formula	Heat of combustion (kJ/mol)[a]	Onset combustion temperature (°C)	ΔH (J/g)	No. of moles			
					Fuel	CO_2	N_2	H_2O
Urea	CH_4N_2O	636	327	265	5	5	8	10
Glycine	$C_2H_5NO_2$	980	186	1496	10/3	20/3	14/3	25/3
HMT	$C_6H_{12}N_4$	4215	280	685	5/6	5	14/3	5

[a]Reference 16.

Huey HNO_3, 65 wt %) to obtain $Y(NO_3)_3$. After the exothermic reaction cooled, the nitrate solution was equally divided into six crucibles. The amount of $Bi(NO_3)_3 \cdot XH_2O$ (Alfa Aesar, Puratronics, 5N), with X assumed to be 6, was calculated with respect to the mass of Y_2O_3 per crucible (3 g) to yield the desired dopant concentration [67 mg of $Bi(NO_3)_3 \cdot 6H_2O$ corresponds to 1 mol % doping] and added to the crucibles. The substitutional doping of Bi ranged from 0.1 to 15 mol %. After this gentle exothermic reaction cooled, a fixed amount of fuel, 4.3 g of glycine (Fisher, reagent grade), 5.2 g of urea (Baker analyzed reagent grade), or 2.0 g of HMT (Fisher, certified A.C.S.) were added to each crucible and thoroughly mixed. The amount of fuel was calculated to be 30% excess of the stoichiometric amount assuming full combustion of the starting material: $2Y(NO_3)_3 + fuel \rightarrow Y_2O_3 + CO_2 + N_2 + H_2O$, where Table I presents the coefficients for the balanced equation for the production of 1 mol of Y_2O_3 for each fuel. Prior to combustion, the mixture was dried in a vacuum oven at 115 °C for 18 h. Combustion of all samples was conducted in air using a muffle furnace set at 600 °C. After the combustion process, inhomogeneous dark-colored nanopowders were obtained. Annealing at 1000 °C for 1 h in air generated homogeneously white nanopowders.

Pre- and postcombusted materials were investigated by differential scanning calorimetry (DSC) using a PerkinElmer diamond instrument. The temperature ranged from 100 to 600 °C with 20 °C/min heating rate. Structural characterization was carried out using a Siemens D5000 x-ray diffractometer with Cu $K\alpha$ radiation.

Transmission electron microscopy (TEM) was performed using a JEOL 3000F high resolution TEM operating at 300 keV accelerating voltage. Samples were crushed between two glass slides and swiped onto 400 mesh carbon-coated Cu grids (SPI, Inc.). Dark field images were acquired using an aperture large enough to contain several diffraction spots.

PL excitation (PLE) and emission (PL) measurements were obtained in ambient conditions using a Photon Technology International TimeMaster™ fluorimeter. RL measurements were carried out in vacuum at room temperature using a Mo-target x-ray source operating at 50 kV and 40 mA. The effective x-ray energy was ~25 keV and the dose rate at the sample was 1.75 Gy/s (measured in air).

TL experiments were carried out on a Risø TL/OSL DA-15 automated system. The samples were affixed to stainless steel disks using silicone spray, and irradiations were performed with an on-board $^{90}Sr/^{90}Y$ β irradiation source delivering 0.13 Gy/s calibrated with quartz. Total doses from 0.4 to 99 Gy were used. The samples were heated at a rate of 1 °C/s and light detection was accomplished via a photomultiplier tube with bialkali photocathode (Thorn-EMI 9235QA) combined with a Schott BG39 filter (350–600 nm).

III. RESULTS AND DISCUSSION

A. Synthesis and microstructure

SCS is a robust technique that is based on exothermic redox reactions that undergo self-sustaining combustion. Mixtures of metal nitrates (oxidizers) and a fuel undergo spontaneous combustion under heating and the chemical energy from the exothermic reaction heats the precursor mixture to high temperatures promoting chemical bonding among the elemental constituents and crystallization. Given the far-from-equilibrium fast formation time of the nanocrystals, it is not uncommon to obtain metastable materials by SCS.[17]

Y_2O_3:Bi was produced by SCS using three different fuels (urea, glycine, and HMT) and the as-prepared nanopowders were characterized by x-ray diffraction (XRD) and TEM. The combustion process was investigated by DSC measurements of precombusted mixtures of fuel, $Y(NO_3)_3$, and 1 mol % of $Bi(NO_3)_3 \cdot 6H_2O$ in relation to Y_2O_3. Figure 1 presents DSC results for all the three mixtures. The peak originates in the exothermic reaction, being negative since this technique measures the difference in the amount of heat needed to increase the temperature of the sample in relation to a known reference as a function of temperature. Consequently, the intense release of energy during combustion is seen as a negative peak. The variation in the enthalpy of combustion (ΔH) was extracted from the peak area and is presented in Table I. The results showed ΔH to increase from urea to HMT to glycine, with a concomitant decrease in the onset combustion temperature. DSC measurements of postcombusted materials showed no evidence of residual fuel in the SCS products.

TEM images of as-prepared nanopowders using all the three fuels are presented in Fig. 2. Results from materials obtained using urea are presented in Figs. 2(a)–2(c), glycine in Figs. 2(d)–2(f), and HMT in Figs. 2(g)–2(i). In addition to high-resolution imaging [Figs. 2(b), 2(e), and 2(h)], visualization of individual nanocrystals was also obtained by means of dark-field imaging [Figs. 2(c), 2(f), and 2(i)]. TEM results show that the morphology [Figs. 2(a), 2(d), and 2(g)],
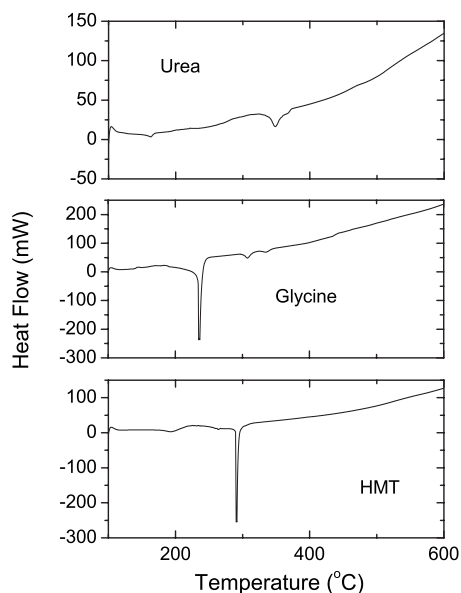
FIG. 1. DSC results of the combustion of Bi-doped $Y(NO_3)_3$ with different fuels.

size, and organization of the crystalline domains [Figs. 2(c), 2(f), and 2(i)] differ considerably for each fuel. Nanopowders produced using HMT and glycine present well-formed faceted individual nanocrystals [Figs. 2(e), 2(f), 2(h), and 2(i)] fused to each other forming large particles [Figs. 2(d) and 2(g)], while those produced using urea [Figs. 2(b) and 2(c)] do not present well-defined crystalline domains. Also clear from the dark-field images is the increase in the average crystallite size from urea to glycine to HMT.

XRD results of SCS-produced materials using different fuels showed Y_2O_3 to have cubic structure,[27] in agreement with the previous results obtained on SCS-produced Tb-
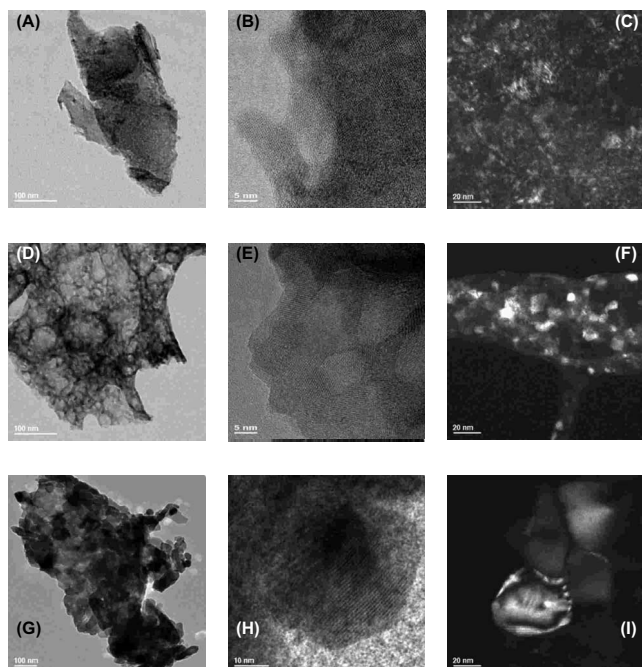

FIG. 2. TEM images of nanopowders prepared using [(a)–(c)] urea, [(d)–(f)] glycine, and [(g)–(i)] HMT. Images (c), (f), and (i) were obtained in dark field mode.
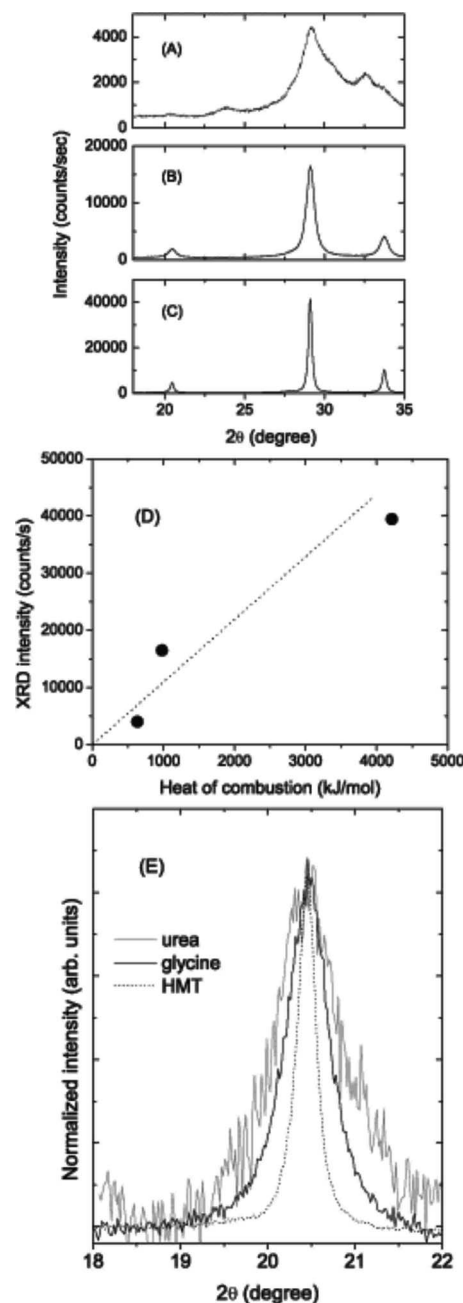

FIG. 3. XRD results of as-prepared nanopowders using (a) urea, (b) glycine, and (c) HMT. (d) Correlation between crystallinity and heat of combustion of SCS fuels, where the line is a guide to the eyes only and (e) diffraction peak broadening due to reduced crystallite size effects in $Y_2O_3:Bi$ (2 mol %) prepared by SCS using different fuels.

doped Y_2O_3,[14] while the presence of Bi_2O_3 (Ref. 28) was observed only in materials prepared using urea. XRD measurements carried out in identical ways using pellets of the same dimensions and mass showed considerable variation in the crystallinity of the samples as a function of fuel. We used the relative intensity of the (222) diffraction peak at 29.1° after background subtraction to infer the degree of crystallinity of each nanopowder. Intensity increased by factors of 4 and 10 for glycine and HMT, respectively, in relation to urea [Figs. 3(a)–3(c)], and a correlation between the heat of combustion of the fuel and crystallinity is shown in Fig. 3(d). These measurements also revealed peak broadening due to
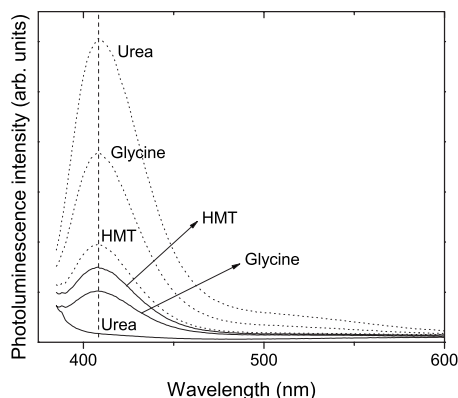
FIG. 4. Comparison of PL spectra excited at 373 nm for as-prepared and 1000 °C annealed samples. The vertical dashed line is a reference to the peak position for all the spectra.

reduced crystallite size effects [Fig. 3(e)], and Debye–Scherrer analysis yielded average sizes increasing from 9 to 13 to 29 nm for urea, glycine, and HMT, respectively. Size analysis of nanopowders annealed at 1000 °C for 1 h yielded similar average crystallite sizes within the 30–35 nm range for all fuels, while the relative intensity of the (222) diffraction peak was 9, 7, and 13 times greater for urea, glycine, and HMT, respectively, in relation to the intensity of the as-prepared nanopowder using urea. Major crystallinity enhancement was observed after annealing of urea- and glycine-prepared nanopowders, where an increase by factors of 9 and ~2, respectively, was observed. Annealing of HMT-prepared nanopowder led to a relatively little change in crystallinity. Additionally, annealing promoted the dissolution of the Bi oxides present in the urea-prepared nanopowder as expected due to the much higher heat of formation of Y_2O_3 than that of Bi_2O_3 at 1000 °C.[18]

B. Luminescence

PL results of as-prepared 2 mol % doped nanopowders excited at 373 nm are presented in Fig. 4, together with those obtained from samples annealed at 1000 °C for 1 h. Within the instrumental resolution of ±1 nm, no shift in the position of the emission band was observed as a function of the fuel, and thus of nanocrystal size or annealing procedure. This is expected since the electronic transitions responsible for PL occur within the Bi^{3+} ion and thus are not quantum confined by the nanocrystals. For the as-prepared nanopowders, HMT yields the highest PL output followed by glycine, while no emission from urea-prepared nanopowder could be detected. On the other hand, annealing reversed this picture by making urea-prepared the brightest nanopowder followed by glycine and HMT. The PL results showed that annealing of SCS-prepared materials leads to the enhancement in luminescence output. It has been suggested that this enhancement originates in the removal of OH^- radicals.[19] In this work, we obtained evidence that improvement of PL output can also be related to increased crystallinity. This is particularly true for the nanopowder prepared using urea as the fuel since PL emission occurred only after annealing. In this case, as shown by XRD results, dissolution of the Bi_2O_3 phase due to annealing leads to the substitution of Bi^{3+} for Y^{3+} and thus to
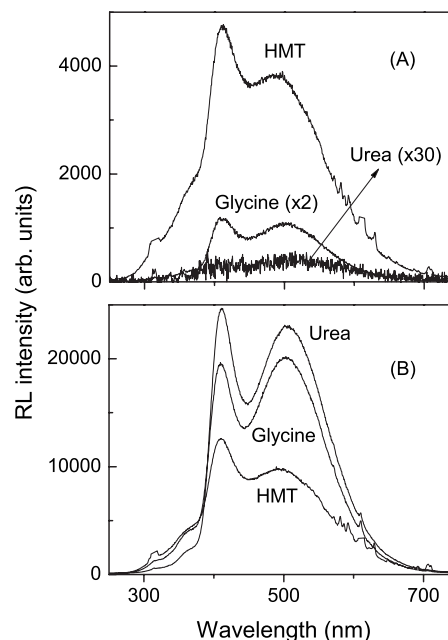

FIG. 5. RL spectra for (a) as-prepared and (b) 1000 °C annealed nanopowders prepared with different fuels.

luminescence activation. Similar results were obtained by means of RL measurements as shown in Fig. 5(a) for the as-prepared and in Fig. 5(b) for the 1000 °C annealed nanopowders. In the case of x-ray excitation, a very weak RL signal from the as-prepared nanopowder using urea as fuel was observed.

Our results show a correlation between crystallinity and PL/RL output since increases in PL/RL output correspond to increases in the (222) diffraction peak intensity. For example, the intensity of the (222) peak increased 1.7 and 1.3 times after annealing for glycine and HMT, respectively, concomitant with increases of 4.3 and 1.4 times in PL and 36 and 2.6 times in RL, respectively. Since structural disorder and the presence of defects may create electronic levels that quench luminescence, PL/RL output enhancement was attributed to the elimination of quenching centers due to increasing nanopowder crystallinity and by the activation of Bi^{3+} centers induced by annealing. Similar results were observed in SCS-prepared Gd_2O_3:Eu.[17]

As discussed in Sec. I, there are two nonequivalent sites for the luminescent center Bi^{3+} ions. Measurements of the excitation and emission spectra of the two centers were carried out for annealed nanopowders doped with 2 mol % prepared using the three fuels (Fig. 6). The center with S_6 symmetry has excitation and emission bands centered at 373 and 408 nm, respectively, while the center with C_2 symmetry has excitation and emission bands centered at 340 and 505 nm, respectively. The excitation and emission peak positions did not vary as a function of the fuel and thus of average crystallite size or degree of crystallinity. This result shows that changes in PL output are related to changes in the number of active recombination centers. The Stokes shifts were calculated to be 0.28 and 1.19 eV for the S_6 and C_2, respectively, slightly smaller (~0.4 eV) than those reported for the bulk.[5] Previous works reported S_6 emission in the range of 405–412
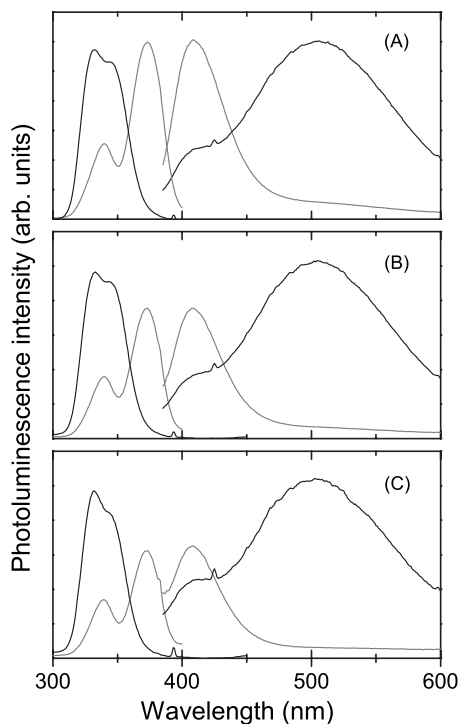
FIG. 6. PL and PLE spectra of 1000 °C annealed Y_2O_3:Bi (2 mol %) nanopowders prepared using (a) urea, (b) glycine, and (c) HMT as the SCS fuel.

FIG. 7. Concentration quenching curve of 1000 °C annealed Y_2O_3:Bi prepared by SCS using glycine as fuel for both emission bands (a) 408 and (b) 505 nm.

nm, while emission from the C_2 center was reported in a broader range, from 481 to 520 nm,[2,3,5–8] though more consistently at 520 nm.[2,5,8] Our results fall comfortably in the reported range of emission values, with the C_2 center emission being very close to the value reported by Toma *et al.*[7] The reason for the larger variation in the reported values of the emission from C_2 centers is not known.

Also seen in Fig. 6 is a systematic decrease in the intensity of the excitation and emission bands related to S_6 sites in relation to C_2 site bands for higher heats of combustion, i.e., from urea [Fig. 6(a)] to glycine [Fig. 6(b)] to HMT [Fig. 6(c)]. Since the C_2:S_6 site population ratio is 3:1, results obtained with HMT are closer to those reported for bulk crystals. These results are in agreement with the theoretical predictions based on atomic-scale simulations of the occupancy of Bi^{3+} in Y_2O_3 using Born-type ions interacting through the Buckingham potential.[20] These calculations suggest that Bi^{3+} ions will preferably occupy S_6 sites but that the high temperatures and lengthy thermal treatments needed to synthesize bulk Y_2O_3 single crystals can overwhelm the potential barrier for C_2 occupancy and populate both sites with equal probabilities.[21] Similarly, progressively more vigorous combustions obtained using urea, glycine, and HMT lead to the population of both sites with more even probabilities and thus to an increase in the number of C_2 sites occupied by Bi ions. Changes in the occupancy of dopants in different crystallographic sites in combustion-prepared phosphors have been reported before.[22] The experimental results obtained in this work demonstrate that the far-from-equilibrium conditions of the SCS method can be explored to obtain unique luminescent properties.
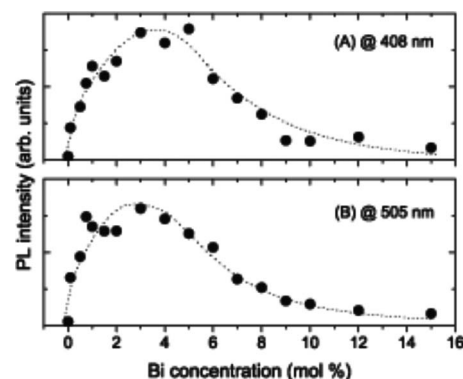
The concentration quenching curve for both emission bands was determined for nanopowders prepared using glycine as fuel after 1000 °C annealing, with Bi concentrations up to 15 mol %. The results are shown in Fig. 7, where the dotted lines are guides to the eyes only. Maximum PL output is observed at around 3 mol %, higher than previously reported for the bulk,[9] and in agreement with the trend commonly observed in nanophosphors.[12,13,23,24] Concentration quenching originates in efficient energy transfer between dopant ions ("dopant chain"), followed by the occasional transfer to a quenching center where energy is lost as heat. In a homogeneously doped bulk crystal, due to the absence of physical boundaries between the dopants, luminescence is maximized at dopant concentrations as high as a few at. %. However, given the large number of nanocrystals forming the nanopowders ($\sim 10^{16}$/g for nanoparticles with 30 nm average size), it has been suggested that in some nanocrystals the dopant chain may happen to be far from the quenching centers, allowing higher concentrations of dopants to be incorporated before quenching is observed.[13]

TL measurements probe a class of defects with energy levels in the band gap of insulating or semiconducting materials. This technique was used to study unannealed 2 mol % Bi-doped Y_2O_3 nanopowders prepared with different fuels. These results are presented in Fig. 8 for the three fuels as a function of irradiation dose. The results were normalized by sample mass to allow for direct comparison between the plots. Spectra analysis shows that there is no shift in the peak temperature of the major TL peaks as a function of irradiation dose, suggesting a first order kinetics TL mechanism. The results also show that for a given irradiation dose, the TL response is progressively more intense for urea-, glycine-, and HMT-prepared nanopowders. The TL spectra of all nanophosphor samples present at least three peaks between 50 and 300 °C, with the peak positions depending on the SCS fuel and the same peaks not being present in all samples. Samples prepared with urea have peaks at 84, 145, and 186 °C, while samples prepared with glycine and HMT have peaks at 87, 162, and 263 °C, and 110, 138, and 250 °C, respectively. Since TL results of bulk Y_2O_3 obtained with a heating rate of 0.32 °C/s (Ref. 25) and of SCS-prepared undoped Y_2O_3 measured at 5 °C/s show two peaks at 115 and 190 °C, 111 and 172 °C, respectively, our results
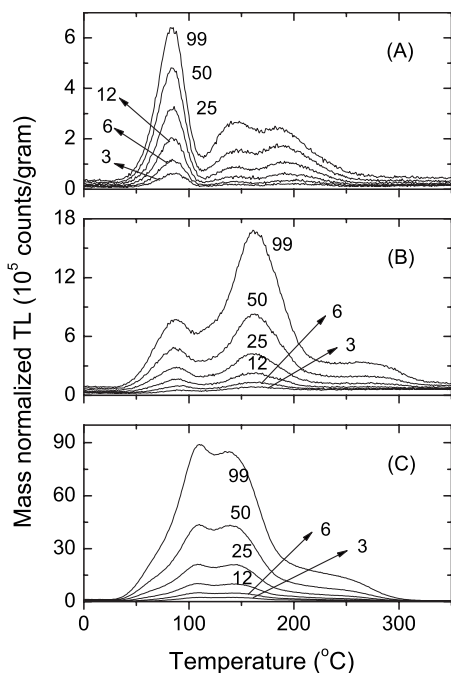
FIG. 8. TL results of Y_2O_3:Bi (2 mol %) as a function of irradiation dose prepared using (a) urea, (b) glycine, and (c) HMT as fuels.

suggest that the incorporation of Bi^{3+} ions is responsible for the creation of additional electron traps. Additionally, the presence of TL peaks at different temperatures in each sample reflect the nonstochastic nature of the combustion process in creating different defects with different concentrations for different synthesis conditions. While the TL peaks of bulk Y_2O_3 have been analyzed using a general-order kinetics model from which activation energies of 1.19 and 1.21 eV were extracted, the nature of the defects and/or impurities generating these traps was not identified.[25] Although further work is necessary to describe in detail the energy of the traps in the nanopowders, the similarity of certain peaks in the nanopowders and bulk samples suggests that the defects responsible for the traps may be similar while having slightly different energy depths below the conduction band due to synthesis conditions and/or structural disorder. In Fig. 9, the integrated TL signal obtained for three different irradiation doses, 3, 25, and 99 Gy, is presented as a function of the heat of combustion of the fuels, showing a correlation between
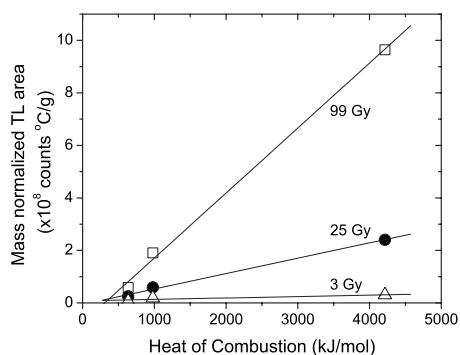

FIG. 9. Correlation between mass normalized integrated TL area and heat of combustion of SCS fuel for several irradiation doses. Line is a guide to the eyes only.

TL area and the amount of energy released during the combustion (heat of combustion). Based on the results presented in Fig. 3(d), it is also possible to correlate the increase in TL with the increase in nanopowder crystallinity. The increase in PL with crystallinity is understood by the activation of Bi^{3+} ions in the host and the elimination of quenching centers leading to the increase in the concentration of active recombination centers. The increase in RL and TL is compatible with the increase in the concentration of recombination centers,[26] though direct measurement of the concentration of traps is needed to fully validate our hypothesis.

IV. SUMMARY AND CONCLUSIONS

The synthesis, structural, and morphological characterization of Bi-doped Y_2O_3 nanopowders produced by SCS together with luminescence investigation were carried out. By means of XRD, PL, and RL measurements, a correlation between crystallinity and luminescence output was determined. Such correlation is attributed to the progressive activation of Bi^{3+} ions in the host and the elimination of quenching centers. It was also found that Bi^{3+} occupancy in the C_2 and S_6 sites and the dominant luminescence emission wavelength can be controlled by the synthesis conditions (fuel), and that maximum PL output was found for 3 mol % dopant concentration. Additionally, TL signal was found to increase for nanopowders prepared using fuels with higher heats of combustion and thus increasing crystallinity of the nanopowders. Most likely, increases in RL and TL are also due to the increase in the concentration of recombination centers.

[1]W. M. Yen and M. J. Weber, *Inorganic Phosphors* (CRC, Boca Raton, FL, 2004).
[2]G. Boulon, J. Phys. (Paris) **32**, 333 (1971).
[3]G. Blasse and A. Bril, J. Chem. Phys. **48**, 217 (1968).
[4]F. Réal, V. Vallet, J.-P. Flament, and J. Schamps, J. Appl. Phys. **127**, 104705 (2007).
[5]A. M. van de Craats and G. Blasse, Chem. Phys. Lett. **243**, 559 (1995).
[6]S. Z. Toma and D. T. Palumbo, J. Electrochem. Soc. **116**, 274 (1969).
[7]S. Z. Toma and D. T. Palumbo, J. Electrochem. Soc. **117**, 236 (1970).
[8]O. M. Bordum, Zh. Prikl. Spektrosk. **69**, 60 (2002).
[9]R. K. Datta, J. Electrochem. Soc. **114**, 1137 (1967).
[10]Y. Tao, G. Zhao, X. Ju, X. Shao, W. Zhang, and S. Xia, Mater. Lett. **28**, 137 (1996).
[11]G. Tessari, M. Bettinelli, A. Speghini, D. Ajo, G. Pozza, L. E. Depero, B. Allieri, and L. Sangaletti, Appl. Surf. Sci. **144–145**, 686 (1999).
[12]M. A. Flores-Gonzalez, G. Ledoux, S. Roux, K. Lebbou, P. Perriat, and O. Tillement, J. Solid State Chem. **178**, 989 (2005).
[13]R. E. Muenchausen, L. G. Jacobsohn, B. L. Bennett, M. A. McKigney, J. F. Smith, J. A. Valdez, and D. W. Cooke, J. Lumin. **126**, 838 (2007).
[14]J. J. Kingsley and K. C. Patil, Mater. Lett. **6**, 427 (1988).
[15]L. A. Chick, L. R. Pederson, G. D. Maupin, J. L. Bates, L. E. Thomas, and G. J. Exarhos, Mater. Lett. **10**, 6 (1990).
[16]*CRC Handbook of Chemistry and Physics*, 60th ed., edited by R. C. Weast (CRC, Boca Raton, FL, 1980), pp. D283.
[17]L. G. Jacobsohn, B. L. Bennett, R. E. Muenchausen, S. C. Tornga, J. D. Thompson, O. Ugurlu, D. W. Cooke, and A. L. Lima Sharma, J. Appl. Phys. **103**, 104303 (2008).
[18]*The Oxide Handbook*, edited by G. V. Samsonov (IFI/Plenum Data Co., New York, 1982), p. 32.

[19] E. Zych, Opt. Mater. **16**, 445 (2001).
[20] C. R. Stanek, K. J. McClellan, M. R. Levy, and R. W. Grimes, IEEE Trans. Nucl. Sci. **55**, 1492 (2008).
[21] C. R. Stanek, K. J. McClellan, B. P. Uberuaga, K. E. Sickafus, M. R. Levy, and R. W. Grimes, Phys. Rev. B **75**, 134101 (2007).
[22] G. Concas, G. Spano, E. Zych, and J. Trojan-Piegza, J. Phys.: Condens. Matter **17**, 2597 (2005).
[23] W. Zhang, P. Xie, C. Duan, K. Yan, M. Yin, L. Lou, S. Xia, and J.-C. Krupa, Chem. Phys. Lett. **292**, 133 (1998).
[24] Z. Wei, L. Sun, C. Liao, C. Yan, and S. Huang, Appl. Phys. Lett. **80**, 1447 (2002).
[25] M. S. Jahan, D. W. Cooke, W. L. Hults, J. L. Smith, B. L. Bennett, and M. A. Maez, J. Lumin. **47**, 85 (1990).
[26] S. W. S. McKeever and R. Chen, Radiat. Meas. **27**, 625 (1997).
[27] PDF File No. 41–1105.
[28] PDF File No. 41–1449.